Super Resolution Phenomenon in the Detection of Buried Objects [0]

Tie Jun Cui[1)], Weng Cho Chew[2)], X. X. Yin[1)], Qin Jiang[1)] and Wei Hong[1)]

[1)] Center for Computational Electromagnetics and State Key Laboratory of Millimeter Waves, Department of Radio Engineering, Southeast University, Nanjing 210096, P. R. China. Email: tjcui@seu.edu.cn.

[2)] Center for Computational Electromagnetics and Electromagnetic Laboratory, Department of Electrical and Computer Engineering, University of Illinois at Urbana-Champaign, Urbana, IL 61801-2991.

I. Introduction

One criterion to evaluate the quality of inverse scattering methods is the resolution of imaging. Classically, the resolution of a wave measured in the far-field regime with limited angles is around 0.5 wavelength according to the Rayleigh criterion. For the linear inverse scattering methods, the image resolution from the far-field data has been limited to 0.5 wavelength [1]. The near-field optical and acoustic microscopy, however, allows this resolution limit to be exceeded. Usually, the image resolution which is less than 0.25 wavelength is called the super-resolution phenomenon.

In this work, we will study the resolution of image quantitatively and the physical reason for super-resolution phenomenon. The study has demonstrated that the information of evanescent waves in the measurement data and involved in the inversion algorithms is the main reason for super resolution. This is because high spatial frequency components of the object are contained in the evanescent waves. Four inversion algorithms are considered to study the super-resolution phenomenon in the half-space problem: the diffraction tomographic (DT) algorithm, the Born approximation (BA) method, the Born iterative method (BIM), and the distorted Born iterative method (DBIM). Further analysis shows that DBIM provides a better super resolution than BIM, and BIM provides a better super resolution than BA. Numerical simulations validate the above conclusions.

II. Study of Resolution in Far-Field Imaging

Consider a general case of a half-space problem. The upper space (region a) and the lower space (region b) are characterized by the relative permittivity $\epsilon_{a,b}$ and the conductivity $\sigma_{a,b}$, respectively. Usually, region a is the air ($\epsilon_a = 1$ and $\sigma_a = 0$) and region b is the earth. The objects to be imaged are located in region b, with relative permittivity ϵ_s and conductivity σ_s. The difference of the complex permittivity $O(\boldsymbol{\rho}) = \tilde{\epsilon}_s(\boldsymbol{\rho}) - \tilde{\epsilon}_b$ forms the object function. If $\epsilon_b = \epsilon_a$ and $\sigma_b = \sigma_a$, the half-space problem becomes a homogeneous-space problem. In this paper, we only consider two-dimensional (2D) dielectric objects. But the results and conclusions can be easily extended to the three-dimensional problem.

To study the possible resolution of image in the inversion of far-field data using the DT algorithm, two kinds of excitations are considered: TM polarized plane waves as incident waves and 2D point sources in the far-field regime as transmitters. The scattered electric fields can be measured along a line parallel to the air-earth interface.

[0]This work was supported in part by the National Science Foundation of China for Distinguished Young Scholars under grant 60225001, P. R. China, in part by the Department of Energy grant DOE DEFG07-97ER 14835, USA, in part by the Air Force Office of Scientific Research under MURI Grant F49620-96-1-0025, USA, and in part by the National Science Foundation under grant NSF ECS 99-06651, USA.

In the DT algorithm, a linear relation is found between the object function and the scattered electric field in the spectral domain [1-3]. Based on the quantitative study of the object spectrum in various far-field measurement setup, we obtain a region where the object function is defined in the spectral domain. Hence, the resolution in far-field imaging can be accurately determined. For the case of a homogeneous space, under the incidence of a plane wave, the resolution of image is $0.5\lambda_a$ if the measurement line is perpendicular to the incident direction while the incident angle rotates from 0 to 2π. If the measurement line keeps unchanged while the incident angle varies from 0 to 2π, however, the resolution of image becomes $0.3536\lambda_a$. Under the excitation of multiple point-source transmitters, the resolution of image is $0.3536\lambda_a$ if multiple receivers are placed on both sides of the object. For the half-space detection problem, only the object spectrum in a fan-shaped region can be determined in the spectral domain under the plane-wave incidence or point-source excitation. Such spectrum is insufficient to get the object function in the spatial domain. Hence, the DT algorithm cannot be used to reconstruct the object in a half space from the far-field data.

III. Super Resolution in Near-Field and Nonlinear Imaging

Now we consider the half-space detection problem under the excitation of point sources. If both the transmitters and receivers are in the near-field region, evanescent waves are captured in the scattered field. Based on the accurate analysis, the evanescent waves $k_a \leq |k_x| \leq k_b$ for the upper half space are used to determine the object spectrum in the DT algorithm. Here, k_a and k_b are wave numbers in regions a and b. With multiple transmitters, multiple receivers and multiple frequencies, the object spectrum in a circle region is obtained, which is centered at the origin with radius $2k_b$ in the spectral domain. Hence, the spatial resolution of the object function is as small as $0.5\lambda_a/\sqrt{2\epsilon_r}$, where $\epsilon_r = \epsilon_b/\epsilon_a$. Typically, $\epsilon_r > 4$ for sand and soil. Therefore, the spatial resolution is less than 0.1768 wavelength in the near-field detection using the DT algorithm.

However, only a small portion of the evanescent waves ($k_a \leq |k_x| \leq k_b$) is captured in the DT algorithm. Although the evanescent waves when $|k_x| > k_b$ are contained in the near-field measurement data, they cannot be used in the DT algorithm because they provide the object spectrum in a complex plane. To produce a better resolution, we directly consider the following nonlinear integral equation in the spatial domain

$$E_a^s(\boldsymbol{\rho}_r, \boldsymbol{\rho}_t) = k^2 \int_{\mathcal{D}} d\boldsymbol{\rho} g_{ab}(\boldsymbol{\rho}_r, \boldsymbol{\rho}) E_b(\boldsymbol{\rho}, \boldsymbol{\rho}_t) O(\boldsymbol{\rho}), \tag{1}$$

where E_a^s is the scattered field at the receiver location, g_{ab} is the half-space Green's function, E_b is the internal field inside the buried object, and O is the object function. If the internal field E_b is replaced by the incident field E_b^{inc}, which is generated by the point-source transmitter, (1) is linearized and can be solved using the Tikhonov regularization method [4]. Because the evanescent waves beyond $|k_x| > k_b$ are captured in both g_{ab} and the incident field correctly, a much better supper resolution is expected for the near-field imaging from the BA method.

For validation, we consider a lossy half-space problem: $\epsilon_a = 1$, $\sigma_a = 0$, $\epsilon_b = 4$ and $\sigma_b = 1$ mS/m. The reconstruction domain 4×2 m^2 is discretized by 64×32 pixels. Under the working frequency of 100 MHz, the size of buried targets is only $\lambda_a/12$. When 50 transmitters and 50 receivers are placed on the air-earth interface, the reconstruction results from BA is illustrated in Figure 1. Clearly, a resolution of at least $\lambda_a/24$ is achieved using BA. Obviously, this is a super resolution. From the above discussion, the evanescent waves involved in (1) is the physical reason for the super resolution, because they contain the information of high-frequency components of the object function. If we remove the evanescent waves from (1), it will be equivalent to the far-field detection. In this case, the reconstructed results of the same problem are shown in Figure 2. Obviously, very

poor resolution images are obtained, where three buried targets cannot be distinguished. This example validates the conclusion that evanescent waves are the main reason for the super resolution.

Instead of using E_b^{inc} to replace E_b, we compute the internal field by a fast forward solver based on the reconstructed object function from BA. Then (1) becomes a linear integral equation, from which the object function can be updated. Repeating the procedure yields the Born iterative method. To obtain the internal field, the following electric field integral equation (EFIE) has to be solved

$$E_b(\boldsymbol{\rho}, \boldsymbol{\rho}_t) - k^2 \int_{\mathcal{D}} d\boldsymbol{\rho}' g_{bb}(\boldsymbol{\rho}, \boldsymbol{\rho}') E_b(\boldsymbol{\rho}', \boldsymbol{\rho}_t) O_0(\boldsymbol{\rho}') = E_b^{\text{inc}}(\boldsymbol{\rho}, \boldsymbol{\rho}_t), \tag{2}$$

where g_{bb} is the half-space Green's function when $\boldsymbol{\rho}$ and $\boldsymbol{\rho}'$ are both in region b. From (2), we clearly see that both propagation waves ($|k_x| \leq |k_b|$) and evanescent waves ($|k_x| > |k_b|$) are contained in the Green's function g_{bb}, which are always involved in the EFIE whether the transmitters and receivers are in the near-field region or far-field region. For the near-field detection, all of g_{ab}, g_{bb} and the incident field contain the information of evanescent waves in BIM. Hence, BIM can provide better supper resolutions than the Born approximation. For the far-field detection, evanescent waves are not involved in the Born approximation, but are captured by g_{bb} in BIM. Physically speaking, the BIM procedure has considered the multiple scattering within the buried objects, which produces more evanescent waves.

The distorted Born iterative method is an efficient nonlinear inverse scattering algorithm [4]. Instead of using the half-space Green's function in (1), an inhomogeneous Green's function G_{ab} is applied in DBIM:

$$E_a^s(\boldsymbol{\rho}_r, \boldsymbol{\rho}_t, O) = E_a^s(\boldsymbol{\rho}_r, \boldsymbol{\rho}_t, O_0) + k^2 \int_{\mathcal{D}} d\boldsymbol{\rho} G_{ab}(\boldsymbol{\rho}_r, \boldsymbol{\rho}, O_0) E_b(\boldsymbol{\rho}, \boldsymbol{\rho}_t, O)[O(\boldsymbol{\rho}) - O_0(\boldsymbol{\rho})]. \tag{3}$$

Here, $O_0(\boldsymbol{\rho})$ is the object function reconstructed from the previous step. It is obvious that (3) is a nonlinear integral equation. If $E_b(\boldsymbol{\rho}, \boldsymbol{\rho}_t, O)$ is replaced by $E_b(\boldsymbol{\rho}, \boldsymbol{\rho}_t, O_0)$, i.e., using the distorted Born approximation, the nonlinear integral equation is linearized, from which the object function can be updated.

The physical significance of the inhomogeneous Green's function G_{ab} implies that the electric field at the receiver location $\boldsymbol{\rho}_r$ produced by a 2D point source located at $\boldsymbol{\rho}$ in the inhomogeneous medium O_0. From the reciprocity theorem, such field should be equivalent to the electric field at $\boldsymbol{\rho}$ in the inhomogeneous medium produced by a 2D point source located at the receiver location $\boldsymbol{\rho}_r$. Hence, both propagating waves and evanescent waves are contained in the inhomogeneous Green's function G_{ab} and the internal electric field E_b whether the transmitters and receivers are placed in the near-field region or far-field region. In other words, the DBIM procedure makes use of more evanescent-wave information than BIM. Thus, DBIM has a better super resolution than BIM, and BIM has a better super resolution than BA. Simulation results shown in Figure 3 validate the above conclusions.

References

[1] E. Wolf, *Opt. Commun.*, vol. 1, pp. 153-164, Sep./Oct. 1969.

[2] A. J. Devaney, *Ultrasonic Imaging*, vol. 4, pp. 336– 360, 1982.

[3] T. J. Cui and W. C. Chew, *IEEE Trans. Geosci. Remote Sensing*, vol. 38, pp. 2033-2041, July 2000.

[4] T. J. Cui, W. C. Chew, A. A. Aydiner and S. Y. Chen, *IEEE Trans. Geosci. Remote Sensing*, vol. 39, pp. 339-346, Feb. 2001.

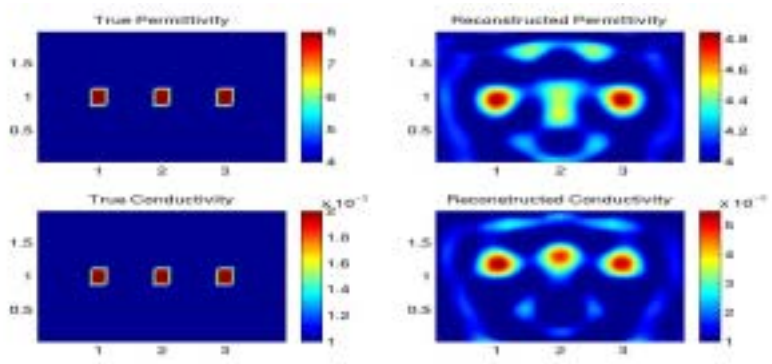

(a) (b)

Figure 1: Original profiles of the buried objects and the reconstructed results using the Born approximation method when the transmitters and receivers are on the air-earth interface. (a) True profiles. (b) Reconstructed results.

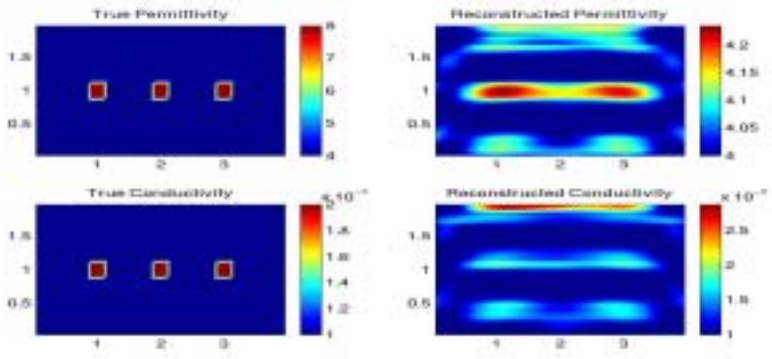

(a) (b)

Figure 2: Original profiles of the buried objects and the reconstructed results using the Born approximation method when the evanescent waves are removed. (a) True profiles. (b) Reconstructed results.

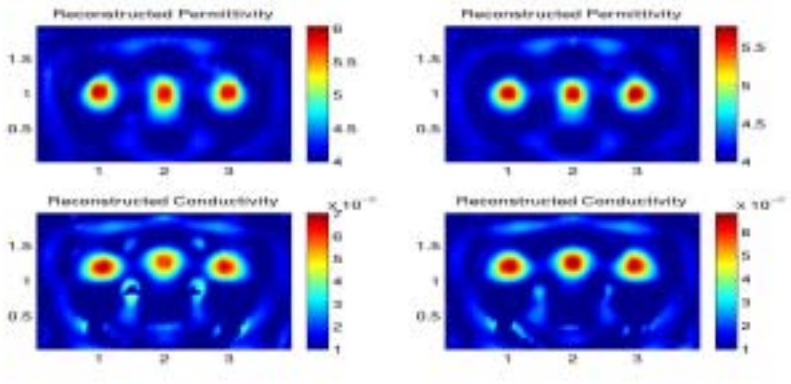

(a) (b)

Figure 3: Reconstructed results using BIM and DBIM when the transmitters and receivers are on the air-earth interface. (a) BIM results after 5 iterations. (b) DBIM results after 5 iterations.